

Information geometry for model identification and parameter estimation in renewable energy – DFIG plant case

ISSN 1751-8687

Received on 12th May 2017

Revised 14th September 2017

Accepted on 6th October 2017

doi: 10.1049/iet-gtd.2017.0606

www.ietdl.org

Andrija T. Sarić¹ ✉, Mark K. Transtrum², Aleksandar M. Stanković³

¹Department of Power, Electronic and Communication Engineering, Faculty of Technical Sciences, Novi Sad, Serbia

²Department of Physics and Astronomy, Brigham Young University, Provo, UT, USA

³Department of Electrical and Computer Engineering, Tufts University, Medford, MA, USA

✉ E-mail: asaric@uns.ac.rs

Abstract: This study describes a new class of system identification procedures, tailored to electric power systems with renewable resources. The procedure described here builds on computational advances in differential geometry, and offers a new, global, and intrinsic characterisation of challenges in data-derived identification of electric power systems. The approach benefits from increased availability of high-quality measurements. The procedure is illustrated on the multi-machine benchmark example of IEEE 14-bus system with renewable resources, but it is equally applicable to identification of other components and systems (e.g. dynamic loads). The authors consider doubly-fed induction generators (DFIG) operating in a wind farm with system level proportional–integral controllers.

1 Introduction

Dynamic models used in analysis of power systems (e.g. electro-mechanical models used in transient analysis) have grown in size to thousands of generators and tens of thousands of nodes. However, this growth in quantitative terms has largely been unaccompanied with improvements in fidelity of predictions. Specifically, models have been largely unable to replicate major system-wide events like the 2003 blackout in the Eastern interconnection [1], and several such events in the 1990's in the Western interconnection [2]. This is even more disturbing, given the relatively widespread presence of sensors that have made detailed recordings during transients.

System identification is particularly lacking in medium-voltage (MV) networks, where much of renewable energy integration is occurring. These ‘active distribution’ networks are evolving at a fast pace because of: (i) changes within (MV lines are relatively easy to build, with potentially more renewables in spatial proximity), (ii) changes above (in transmission – e.g. topology control), and (iii) changes below (more storage, power electronic loads). The increased presence of renewable resources interfaced through power electronic converters has recently led to some qualitatively new stability problems in such networks. The lack of accurate parameter values is common in power systems, because manufacturers do not provide many of the data sets required for analysis. Moreover, parameter values vary under different operating conditions. The deployment of digital fault recorders by the utilities has enabled the use of disturbance recordings for estimation of missing or changed parameters.

The use of operational, on-line data to tune dynamical models of key components [e.g. synchronous generators (SGs)] has a long history in power systems. General dynamical systems concepts like trajectory sensitivity have been introduced more than a quarter century ago [3, 4]. An extension of that particular approach to hybrid systems was presented in [5]. Another influential approach is based on extracting local information from the measurement Jacobian, as described in [6]. To handle the numerical ill conditioning which often accompanies the parameter estimation problem, the reference proposes that a subset of parameters of the model be fixed to prior values, while estimating the remaining parameters from the available data (denoted as the subset selection method). In the sequel, we only list references directly related to our development here. Cari and Alberto [7] considered parameter

estimation for a single generator and formulated the SG identification problem in a differential-algebraic equation (DAE) framework. Huang *et al.* [8] considered the same overall setup, but with phasor measurement unit measurements.

If the sensitivity to the interaction among parameters in a given set is greater than the sensitivity to individual parameters within the same set, the estimation problem is denoted as over-parametrised, and numerical ill-conditioning is to be expected. The performance of parameter estimates depends on the number of uncertain parameters and on available on-line measurements. It is well appreciated by practitioners that optimisation-based approaches to parameter identification often encounter the so-called plateau phenomenon, when the criterion function becomes insensitive over large portions of the parameter space and the problem is characterised by multiple local solutions [9].

In [10], we offer a differential geometric explanation of this phenomenon, based on model manifolds, while in [11] we applied this method for reduction of dynamic models in power systems. In [12], we have presented results of the same analysis on direct-drive SGs (DDSG) and DFIG considered as components individual components. In this paper, we consider the case of DFIG wind farms, with added farm-level controllers that respond to commands issued by the system operator. This is significant, as it has already been shown in [13, 14] that the control loops have dominant influence on the system-wide response of DFIG.

Our dynamic system identification procedure also has implications for steady-state problems in power systems. One example is provided by the conventional power system state estimation, which is essentially a (steady-state) parameter identification problem. Its practical performance has long been plagued by convergence and uniqueness problems [15]. We envision applications of our identification procedure in microgrids, in virtual utilities and energy hubs that are often considered essential for long-term evolution of smart grids, and in future electricity markets where shorter time-scale operation will increase the importance of dynamic model fidelity. It is also important for load modelling, which typically introduces the largest uncertainty in the overall dynamic model.

The outline of the paper is as follows. Section 2 describes the class of power system models considered in identification; Section 3 discusses conditions for well-posedness of parameter estimation, while Section 4 introduces information geometry, a global sensitivity-based approach to model identification; Section 5

describes results obtained for a multi-machine benchmark example; and Section 6 contains our recommendations and conclusions. Appendix provides details for DFIG described by differential and algebraic equations.

2 Power system model for identification

The presence of widely different time scales leads to DAE as the standard form of power system models [16]

$$\frac{dx}{dt} = f(x, z, p, t); \quad (1)$$

$$0 = g(x, z, p, t), \quad (2)$$

where x is the vector of (differential) state variables, z is the algebraic variable, p is the parameter (typically assumed to be unknown in estimation studies) and t is the (scalar) time variable. System measurement vector is assumed to be of the form [6, 7]

$$y = h(x, z, p, t). \quad (3)$$

The parameters (p) are to be estimated from measurements (y); there typically exists prior information about individual parameters, often in the form of plausible ranges for each. The least-squares optimisation formulation of the identification problem is the most prevalent in the literature by far. In that case, the key quantities are parametric sensitivities whose dynamics is described by the following equations:

$$\frac{d}{dt} \frac{\partial x}{\partial p} = \frac{\partial f(x, z, p, t)}{\partial x} \cdot \frac{\partial x}{\partial p} + \frac{\partial f(x, z, p, t)}{\partial z} \cdot \frac{\partial z}{\partial p} + \frac{\partial f(x, z, p, t)}{\partial p}; \quad (4)$$

$$0 = \frac{\partial g(x, z, p, t)}{\partial x} \cdot \frac{\partial x}{\partial p} + \frac{\partial g(x, z, p, t)}{\partial z} \cdot \frac{\partial z}{\partial p} + \frac{\partial g(x, z, p, t)}{\partial p}; \quad (5)$$

$$\frac{\partial h}{\partial p} = \frac{\partial h(x, z, p, t)}{\partial x} \cdot \frac{\partial x}{\partial p} + \frac{\partial h(x, z, p, t)}{\partial z} \cdot \frac{\partial z}{\partial p} + \frac{\partial h(x, z, p, t)}{\partial p}. \quad (6)$$

These equations are linear in terms of sensitivities, but the matrices involved vary along each system trajectory. In the multivariable case, the overall problem dimensionality can grow quickly as, for example, $\partial x / \partial p = [\partial x / \partial p_1 \ \dots \ \partial x / \partial p_i \ \dots \ \partial x / \partial p_p]^T$ and $\partial x / \partial p_i$ is an n -dimensional vector (p is total number of uncertain parameters and n is total number of state variables). Details about DAE modelling of a doubly-fed induction generator (DFIG) and a transmission network are in the Appendix.

3 Parameter estimation

Equation (6) determines the ($m \times p$)-dimensional (m is total number of available measurements) Jacobian matrix $J_p(t) = \partial h(t) / \partial p$, or the matrix of first partial derivatives of system measurement vector (3) with respect to the parameter vector (p) at each time point. In the neighbourhood of true parameter values, the full Hessian matrix of second derivatives is well approximated with $H_p(t) = J_p^T(t) J_p(t)$, which is symmetric and positive semidefinite (all its eigenvalues are real and non-negative). Consider the case when $H_p(t)$ is singular with a single eigenvalue at 0; then the variation of parameters along the corresponding eigenvector cannot be detected from measurements. Typically $H_p(t)$ is not exactly singular, and nearness to singularity is measured by the *condition number* $\kappa(H_p)$, which for a symmetric and positive matrix is the ratio of the largest (λ_{\max}) to smallest eigenvalue (λ_{\min}) [6].

There are important consequences of the Hessian near-singularity. The first is that the solution of DAEs (1) and (2) varies much more slowly in some parameter p directions than in others. The second is that the vector p is poorly estimated in directions where the curvature is small (relative to directions with high curvature). Numerous literatures [3, 6–8] state that all parameters

cannot be estimated together in typical cases. In our work, the ill-conditioned parameters are detected using participation factors of $H_p(t)$ [11].

4 Information geometry, semi-global and global sensitivities

It has been shown recently that for understanding the global properties of models and for advancing numerical techniques for exploring them, it is beneficial to focus on data (measurement) space rather than parameter space [17, 18]. This shift in viewpoint is known as *information geometry*, since it combines *information theory* with *differential geometry*, and it is a natural mathematical language for exploring parameterised models [19]. The foundation of the approach is the interpretation of a model as a manifold embedded in the space of data, known as the model manifold. The key features of the approach are:

- There is no information loss, since the manifold retains information about all model predictions [17, 18]. In contrast, the cost surface in parameter space condenses the high-dimensional quantities such as the prediction and measurement vectors into a single number – the cost.
- Information geometry separates the model (the manifold embedded in data space), from the data to which it is being fit (a point in the data space [17, 18]). This is a useful abstraction, allowing study of intrinsic properties of the model regardless of any particular experimental observation. In contrast, the cost surface in parameter space is a function of, and often very sensitive to, the observation.
- The set of points that constitute the model manifold is the same regardless of possible model re-parameterisations [17–19]. The parameters are not disregarded completely, since they act as coordinates on the manifold.
- The Riemannian metric on the model manifold (describing differences in predictions of two models that are infinitesimally apart) is the Fisher information matrix (FIM), i.e. the Hessian matrix introduced above [17–19]. Information geometry thus naturally connects the local and the global analysis.
- The language of differential geometry naturally accommodates the potentially large dimensionality of both the parameter and the data spaces.

Our procedure complements the more commonly used local parameter sensitivity analyses with semi-global and global techniques. *Semi-global* methods address the inadequacies of local methods by sampling parameter space in a finite neighbourhood around the best fit; standard tools include scanning and Bayesian methods. Information geometry aims to capture the *global* properties of models and to numerically explore them. The main idea is to consider a model as a manifold embedded in the space of data. Since the information geometric approach has been recently described in considerable detail elsewhere, both for the general modelling case [17, 18], as well as for power systems specifically [10, 11], we omit a detailed description here. Instead, we focus on the key quantity that will be used in this paper: *geodesics*.

Geodesics are distance minimising curves, i.e. analogues of straight lines, on curved surfaces. They are found as the (numerical) solution to a second-order ordinary differential equation in parameter space (while utilising quantities from the data space)

$$\frac{\partial^2 p^i}{\partial \tau^2} = \sum_{j,k} \Gamma_{jk}^i \frac{\partial p^j}{\partial \tau} \cdot \frac{\partial p^k}{\partial \tau}; \quad \Gamma_{jk}^i = \sum_{\ell,m} (I^{-1})^{i\ell} \frac{\partial y_m}{\partial p^\ell} \cdot \frac{\partial^2 y_m}{\partial p^j \partial p^k}. \quad (7)$$

where Γ are known as the Christoffel symbols [11], which are expressed in terms of the parametric sensitivities in (4)–(6) and I is the FIM which is well approximated by the Hessian. The parameter τ is the arc length of the geodesic curve as measured on the model manifold, i.e. in data space. Notice how the model provides the connection between the parameter space and data space through the Jacobian matrix $J_p(t) = \partial h(t) / \partial p$ as calculated in (4)–(6). Further

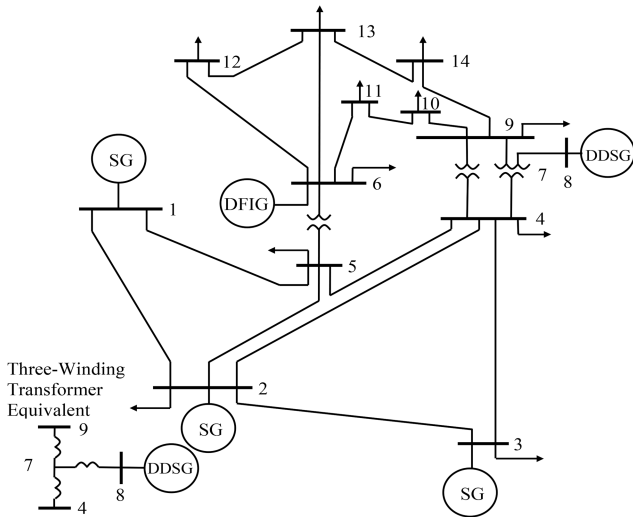


Fig. 1 Modified IEEE 14-bus test system with three types of resources (SG, DFIG, and DDSG)

note that the Christoffel symbols involve the second-order sensitivities that are found by taking another derivative in (4)–(6). We do not give an explicit formula because, although the derivation is straightforward, the result is lengthy and does not give any new insights. Furthermore, because we evaluate these sensitivities using automatic differentiation [11], these expressions are not explicitly needed. There is a technical subtlety in the evaluation of (7) that is critical for our approach to be tractable for large models. As the second derivative of the observation vector is contracted twice with the geodesic velocity vector (i.e. the sums over indices j and k in (7) form two ‘dot products’ with the geodesic velocities and the array of second derivatives), only a directional second derivative is needed, which can be calculated efficiently as in [11].

Solutions to the geodesic (7) are calculated using standard methods for numerically integrating initial value problems. The geodesic is found by first selecting initial parameter values and an initial direction in parameter space ($\partial p/\partial \tau$). In this example, we take these to be the ‘true’ parameter values and the eigenvector of the FIM with smallest eigenvalue (we use quotes to denote that these ‘true’ parameter values are not necessarily the true values used to generate the data; they are the starting point of a geodesic). Our global analysis requires starting from a variety of initial parameter values and directions. Next, we numerically solve the model DAEs (1) and (2), the sensitivities (4)–(6), and the second-order sensitivities in the direction of $\partial p/\partial \tau$. These quantities are used to construct the Jacobian matrix ($J_p(t) = \partial h(t)/\partial p$), the FIM matrix $I = J_p^T J_p$, and the geodesic acceleration (7). Next, we numerically solve (7), evaluating the model equations and first- and second-order sensitivities at each step of the integration. The geodesics extend the parameter identifiability analysis of the MCMC. The geodesic curves are parameterised by the proper distance on the model manifold, i.e. by changes in model behaviour. When geodesic curves extend parameter values to zero or infinity in a finite distance on the model manifold, the corresponding parameter is susceptible to identifiability problems.

A key observation from information geometry is that the model manifold for energy systems (similar to models in many other fields) is bounded. Furthermore, the differential structure on the boundary (i.e. cusps and edges) naturally divides the boundary into a hierarchy of cells. The relevant structure is similar to a polygon – a hierarchy of faces, edges, vertices – generalised to higher dimensions (i.e. a polytope). Unlike a traditional polytope whose faces and edges are flat, the faces and edges of the model manifold are typically curved, but are smooth. The manifold is therefore equivalent to a polytope in the differential topological sense, i.e. equivalent under diffeomorphisms.

The faces of the model manifold occur when parameters can vary over their entire physically allowed range, i.e. take on extreme values, without the model predictions becoming infinite. To

illustrate consider an example in which a dynamical system modelled as a set of differential equations has parameters associated with several relevant time scales, a common occurrence in power systems. The limit in which a single time scale becomes zero, the model becomes a set of differential-algebraic equations through a singular limit. The resulting DAEs model corresponds to a face on the model manifold. An alternative singular limit in which a different time scale becomes zero (leading to a different set of differential-algebraic equations) corresponds to a different face of the model manifold.

The faces of the model manifold are particularly relevant for parameter identifiability analysis. If the observed data are not sufficiently informative, the confidence region may extend to the boundary of the model manifold. Since the manifold boundary maps to extreme values of the parameters, the data effectively place no constraints on the allowed parameter values, i.e. the confidence region of one or more parameters may be infinite. If this is the case, then we say the parameter is practically unidentifiable.

5 Application

We have developed a Matlab-derived simulation environment, which considers stability-related models in the DAEs based form (1) and (2). Our environment is based on PSAT, which is a suite of freely available Matlab routines well documented in [20], to which we have added our code for evaluation of measurement sensitivities (in Matlab) and for computational differential geometry (in Julia). Our Matlab code is general in the sense that it allows for a variety of on-line measurements: rotor angle and speed, nodal active and reactive power injections, nodal voltage magnitude and angle, branch active and reactive flows, and branch current magnitude.

Original IEEE 14-bus test system [20] is modified to include DFIG (capturing prevalent type of wind plants today), DDSG (used by industry to model solar plants and a new generation of wind) and SGs (describing conventional units and interconnections) as shown in Fig. 1. Detailed analyses for SG and DDSG parameter identifiability from the information geometric perspective are presented in [10, 11] and [12], respectively. In this paper, we study DFIG with added farm-level proportional–integral (PI) controllers to achieve responsiveness to system operator requests [13, 14] (please see the Appendix for details).

Input parameters for analysed DFIG are as follows: $V_n = 13.8$ kV, $r_s = 0.01$ pu, $x_s = 0.1$ pu, $r_r = 0.01$ pu, $x_r = 0.08$ pu, $x_\mu = 3$ pu, $H_m = 3$ MWS/MVA, $K_p = 10$, $T_p = 3$ s, $K_v = 10$, $T_e = 0.01$ s, $R = 75$ m, $n_p = 4$, $n_b = 3$, $n_{GB} = 0.01123596$, $P_{max} = 1$ pu, $P_{min} = 0$, $Q_{max} = 0.7$ pu, $Q_{min} = -0.7$ pu, $T_{e2} = 0.005$ s, $k_{p1} = 1$, $k_{i1} = 0.1$, $k_{p2} = 1$, $k_{i2} = 0.1$ and $Q_{ref} = 0.1$, where (other parameters are described in Appendix) K_v is the voltage control gain; R is the rotor radius; N_p is the number of poles; N_b is the number of blades; n_{GB} is the gear box ratio; P_{max} , P_{min} are maximum and minimum active power, respectively; Q_{max} , Q_{min} are maximum and minimum reactive power, respectively.

5.1 Local sensitivity analysis

In the case of DFIG from (8) and (9) each unit (assumed DFIG driven) has six states (ω_m , θ_p , x_1 , i_{rd} , x_2 and i_{rq}) and one algebraic variable [$P_v^*(\omega_m)$]. We classify the uncertain parameters into four groups: (i) electrical (T_e , x_s , x_μ , and T_{e2}), (ii) mechanical (H_m and T_p), (iii) control (k_{p1} , k_{i1} , k_{p2} and k_{i2}), and (iv) setting parameters (Q_{ref}). Available measurements for the DFIG resource are the rotor angle (δ) and speed (ω) [Note that the rotor angle cannot be measured directly. However, the indirect methods where the rotor angle is calculated from on-line measurements of active/reactive powers and voltage in connection point can be applied (e.g. see [21, eq. (8)].), the real and reactive powers (P_g and Q_g , respectively), as well as the terminal voltage magnitude and angle (V and θ , respectively).

In the case of parameter estimation for a single machine from local measurements, we can remove the algebraic equations

(denoted with \mathbf{g} in (9) in Appendix) altogether; the algebraic variables \mathbf{z} (1)–(3) still remain (V, θ for network buses and other for resource units as described above). In order to demonstrate salient features of our method on a model that is relevant, but straightforward enough for tracking key relationships, we focus on the six differential equations on DFIG example (denoted with \mathbf{f} (8) in Appendix).

However, in actual power systems (also in the analysed modified IEEE 14-bus power system test example), there exist additional dynamical components (exciters, automatic voltage regulators, steam/wind turbines etc.), as well as multiple generators and loads in buses. A single DFIG unit described by \mathbf{f} in (8) would see these other differential/algebraic components through variation in the wind power [$P_w^*(\omega_m)$] and in the complex voltage in the point of connection (represented by V and θ). For simplicity, we assume that interface variables for DFIG in bus 6 (that are $P_w^*(\omega_m)$, V_6 and θ_6) are known functions of time. This, of course, is an approximation for a multi-machine system, but it allows direct comparison with numerous references that focus on a single unit.

We start transients in sensitivities following inadvertent opening of the line 2–4 (see Fig. 1), which is reclosed after 200 ms. For example, the transient variations of the voltage magnitude and angle at bus 6 (where DFIG is connected) are $\sim 4\%$ and 20° , respectively. Our repeated analyses with different line opening locations and power system's loading levels have yielded the same qualitative and quantitative results. The issue of robustness of our procedure to changes in measurement structure has been addressed in [11] for the case of SG.

In Table 1 we present the eigenvalues, condition numbers and participation factors for different uncertain parameter sets. The sloppiness of most of the uncertain parameter sets used is clear.

If we consider, for example, the control parameters, it is clear that k_{p2} and k_{i2} are harder to identify, as they dominantly participate in smallest eigenvalues. This is important, as modal analysis from [13, 14] has already established the key importance of control parameters in quantifying wind farm effects on the power system. Please note that [13, 14] have focused on dynamics of the state, while our emphasis is on parameters, providing a complementary set of conclusions. Our global analysis will provide additional insight into root causes of this challenge.

5.2 Semi-global and global analysis

We have generated artificial data for a set of ‘true’ parameter values and performed a Markov Chain Monte Carlo (MCMC) sampling of the posterior distribution for the model fit to the data. Our MCMC sampling was performed using the ‘affine invariant MCMC ensemble sampler’ of Goodman and Weare [22]. For the analysed type of distributed resource (DFIG) projecting the cloud of points onto each pair of parameter axes typically results in a cloud that is not elliptical (see Fig. 2). Deviations from an elliptical cloud indicate that a simple local analysis will not capture many important structural features of the model.

Consider for example, the cloud of the k_{p2} and k_{i2} cross-section (lower-right in Figs. 2 and 3) which we have seen participating significantly in the smallest eigenvalues and that will be the focus of our global analysis below. The Bayesian sampling suggests that both parameters are unidentifiable from below, i.e. they can be taken to zero without a substantial change in the model behaviour. However, these non-identifiabilities are not independent – taking both parameters to zero results in drastic changes to the model's predictions, as seen by the value of the criterion in Fig. 3, lower left. The reason for this is that the cost surface has a long-narrow

Table 1 Condition numbers [$\kappa(\mathbf{H}_p)$], eigenvalues (λ_i), and participation factors (p_{ki}) for characteristic sets of uncertain parameters

| Uncertain parameters | Condition numbers, $\kappa(\mathbf{H}_p)$ | Eigenvalues, λ_i | Participation factors, p_{ki} |
|--|---|--------------------------|--|
| electrical parameters: T_e, x_s, x_μ, T_{e2} | 6.1×10^8 | 8.43×10^7 | 0.0000; 0.0021; 0.0011; 0.9968 |
| | | 8.02×10^7 | 0.0018; 0.1508; 0.8474; 0.0000 |
| | | 2.68×10^{10} | 0.0011; 0.9953; 0.0010; 0.0026 |
| | | 5.21×10^{16} | 0.9974; 0.0000; 0.0026; 0.0000 |
| mechanical parameters: H_m, T_p | ∞ | 0.00 | 0.5000; 0.5000 |
| | | 4.84×10^7 | 0.5000; 0.5000 |
| electrical and control parameters: $T_e, x_s, x_\mu, T_{e2}, k_{p1}, k_{i1}, k_{p2}, k_{i2}$ | 5.95×10^{11} | 86,050 | 0.00; 0.00; 0.00; 0.00; 0.00; 0.00; 0.00; 1.00 |
| | | 251,838 | 0.11; 0.42; 0.07; 0.39; 0.00; 0.00; 0.00; 0.00 |
| | | 2,950,604 | 0.07; 0.25; 0.06; 0.59; 0.01; 0.03; 0.00; 0.00 |
| | | 1.04×10^8 | 0.00; 0.00; 0.00; 0.00; 0.95; 0.05; 0.00; 0.00 |
| | | 3.39×10^9 | 0.00; 0.01; 0.00; 0.01; 0.06; 0.91; 0.01; 0.00 |
| | | 2.67×10^{10} | 0.00; 0.00; 0.00; 0.00; 0.00; 0.00; 0.99; 0.00 |
| | | 8.11×10^{12} | 0.75; 0.24; 0.01; 0.00; 0.00; 0.00; 0.00; 0.00 |
| control parameters: $k_{p1}, k_{i1}, k_{p2}, k_{i2}$ | 9,688,780.7 | 2.54×10^6 | 0.0000; 0.0000; 0.9072; 0.0928 |
| | | 1.14×10^7 | 0.0000; 0.0000; 0.0928; 0.9072 |
| | | 1.19×10^{12} | 0.9072; 0.0928; 0.0000; 0.0000 |
| | | 2.47×10^{13} | 0.0928; 0.9072; 0.0000; 0.0000 |
| control parameters: k_{p2}, k_{i2} | 44.41 | 5,971,094 | 0.9705; 0.0295 |
| | | 265,203,912 | 0.0295; 0.9705 |
| setting parameters: Q_{ref} | 1.00 | 6.43×10^7 | 1.0000 |

canyon that makes a sharp turn near the centre of the k_{p2} and k_{i2} plane in Figs. 2 and 3. Thus, if one carefully tunes k_{p2} , then the parameter k_{i2} becomes unidentifiable and vice-versa. This non-linear effect cannot be described by a covariance matrix, but is clearly visible in the MCMC sampling clouds of Figs. 2 and 3. It is also reflected in the geodesic paths and we consider shortly.

We complement this semi-global analysis with a global analysis based on information geometry. As mentioned above, relevant structures are analogous to faces on a high-dimensional polytope. We identify these faces by numerically constructing multiple geodesics on the model manifold (the process is described in more detail in [10, 11]) originating from random positions and with random velocities on the model manifold. The geodesics terminate at faces of the model manifold. By inspecting the parameter values along the geodesics curves, we infer the limiting case of each manifold face. In this way, we identify all of the faces of the model manifold.

As a simple illustration of how these ideas and concepts come together to produce a useful insight into model behaviour, consider Fig. 3 in which we demonstrate with a pair of parameters for which the non-linearities in the model are particularly pronounced: k_{p2} , k_{i2} . We use the model to generate artificial data. Next, we fix the values of parameters k_{p2} and k_{i2} and vary the remaining parameters to minimise the difference between the model behaviour at the fixed values of k_{p2} and k_{i2} and the artificial data. This process is repeated for different values of k_{p2} and k_{i2} . The colours in Fig. 3 represent the sum of squares difference between the model behaviour and the artificial data at each k_{p2} , k_{i2} value; in statistics language, this is known as a pairwise likelihood profile. The green dots correspond to the Bayesian sampling from Fig. 2. The black lines are geodesic curves originating from the ‘true’ parameters. Notice that the geodesics naturally align with the local structure of the cost function and are therefore attracted to the limits $k_{i2} \rightarrow 0$ and $k_{p2} \rightarrow 0$. Indeed, these two limits correspond to faces on the model manifold.

For the case of the DFIG with eight electrical and control parameters, we identify ten faces, each of which corresponds to a different unidentifiable parameter in the model. We represent these faces as limits. For example, we find that a particular face corresponds to the limit $k_{i2} \rightarrow 0$. This notation indicates that the parameter k_{i2} is unidentifiable from below (notice the agreement with the MCMC sampling above) and that the corresponding reduced model without this parameter is constructed by taking the limit $k_{i2} \rightarrow 0$ with all other parameters are held fixed. Similarly, we find the following faces: $k_{p2} \rightarrow 0$, $T_{e2} \rightarrow 0$, $x_{\mu} \rightarrow \infty$, $x_s \rightarrow 0$, $T_e \rightarrow 0$, $k_{i1} \rightarrow 0$, and $k_{p1} \rightarrow 0$.

The two remaining limits are more subtle and require further explanation. We find the limit $k_{i2} \rightarrow \infty$, $k_{p2} \rightarrow \infty$, and $T_{e2} \rightarrow \infty$. However, these are not three independent limits. Rather, they reflect a structural correlation in the uncertainty of these parameters. To make this explicit, we introduce new parameters $\tilde{k}_{i2} = k_{i2}/T_{e2}$ and $\tilde{k}_{p2} = k_{p2}/T_{e2}$. In this new parameterisation, the limit takes the form $T_{e2} \rightarrow \infty$ with the new parameters \tilde{k}_{i2} and \tilde{k}_{p2} remaining finite. We refer to \tilde{k}_{i2} and \tilde{k}_{p2} as the identifiable combinations. We also find that $k_{i1} \rightarrow \infty$, $k_{p1} \rightarrow \infty$, and $T_e \rightarrow \infty$ with $\tilde{k}_{i1} = k_{i1}/T_{e1}$, $\tilde{k}_{p1} = k_{p1}/T_e$ the identifiable combinations. Sensitivities of time responses of voltage magnitude and angle in DFIG connection bus to parameters of PI controller (k_{p1} , k_{i1} , k_{p2} , and k_{i2}) are illustrated in Fig. 4. Sensitivities of time responses of DFIG output active power to parameters of PI controller (k_{p1} , k_{i1} , k_{p2} , and k_{i2}) are illustrated in Fig. 5. The local analyses tell a complementary story – the Hessian is ill-conditioned (0.8×10^{12}), without a clear gap in the eigenvalues, and the participation factor analysis [16] identifies k_{i2} and T_{e2} as the dominant in the smallest two eigenvalues. Similarly, the subset selection method [6] looks at the singular value decomposition of the Jacobian, and identifies k_{p2} and T_{e2} as the least identifiable parameters.

The two faces described in the previous paragraph are interesting, because they result from a non-linear correlation among the parameters. One of the useful insights to be gained from

MCMC sampling clouds, such as those above, is similar correlations among parameters. As the dimensionality of the parameter space grows, there arises the potential for high-dimensional correlations similar to those described above. It also becomes increasingly difficult to identify these correlations from two (or even three)-dimensional projections. In contrast, the geometric analysis that we describe identifies these correlations in a systematic and scalable way.

The global analysis just described has several features that naturally complement the local and semi-global analysis. We here focus on three key observations. First, the analysis is global. The method identifies all of the potentially unidentifiable parameters. If the same model class is used to model a different unit under different operating conditions, then the local and semi-global analyses must be repeated. In contrast, the global approach identifies all of the potentially unidentifiable parameters that could arise for these scenarios and potentially could be used to guide repeated local or semi-global analysis. Second, the geometric analysis identifies high-dimensional correlations among parameters in a scalable way. Finally, the geometric analysis makes clear that practically non-identifiable parameters are not a pathology that results from a poor model choice or bad data, but is rather an intrinsic consequence of the mechanistic (physucal) structure of the model. It further gives insights into how to construct grey-box, reduced models (a method known as the manifold boundary approximation method, described in [11]) appropriate for a given circumstance.

6 Conclusion

This paper describes a new class of system identification procedures that are well matched to electric power systems with distributed resources. The approach builds on computational advances in differential geometry, and offers a new, global characterisation of challenges that are frequently encountered in identification of dynamic models in electric power systems. In particular, we use information geometry to develop global sensitivity analysis of differential-algebraic equation models for DFIG-based renewable resource with proportional-integral-differential controller which today dominate wind energy systems. Our procedure characterises the key difficulties in identifying the system parameters (especially in the control loop of a wind unit) and quantifies all possibly unidentifiable parameters. It can be used together with [11, 13, 14] to determine low-order equivalent models for wind farms. Our recommendations for identifying models of large systems are conceptually described in [10], with key system modes serving as means to piece together descriptions of subsystems.

7 Acknowledgments

This work was supported by CURENT Engineering Research Center of the National Science Foundation and the Department of Energy under NSF Award Numbers EEC-1041877 and ECCS-1710944, by ARPA_E under contract DE-AR0000223, and in part by the Ministry of Education and Science of the Republic of Serbia, under project III-42004.

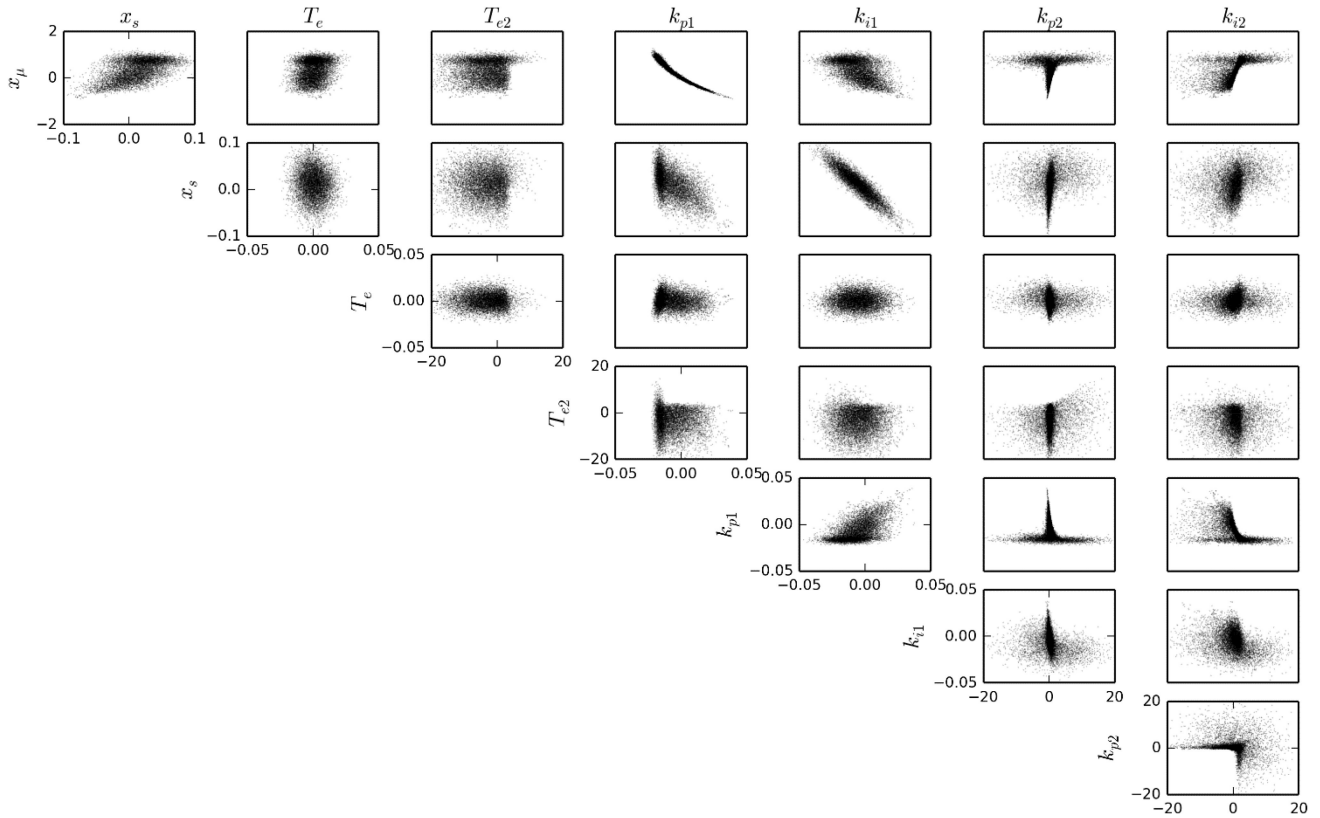


Fig. 2 Point clouds drawn from an MCMC sampling of the posterior distribution showing pairwise correlations among parameters. Clouds that are not elliptical indicate that a simple local analysis will not capture many important structural features in the credible region

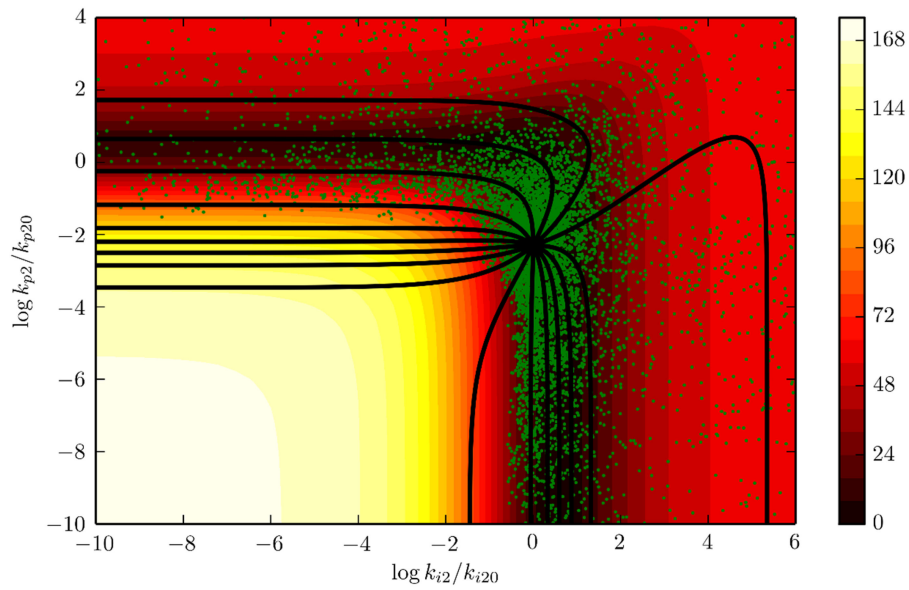


Fig. 3 Illustration of the relationship between likelihood profiles, Bayesian sampling, and model manifold geodesics. The background colour corresponds to the sum of square difference between model behaviour for fixed values of k_{p2} and k_{i2} with the remaining parameters optimised to minimise the difference. Green dots are a Bayesian sampling. Black curves are geodesics originating from the 'true' parameter values

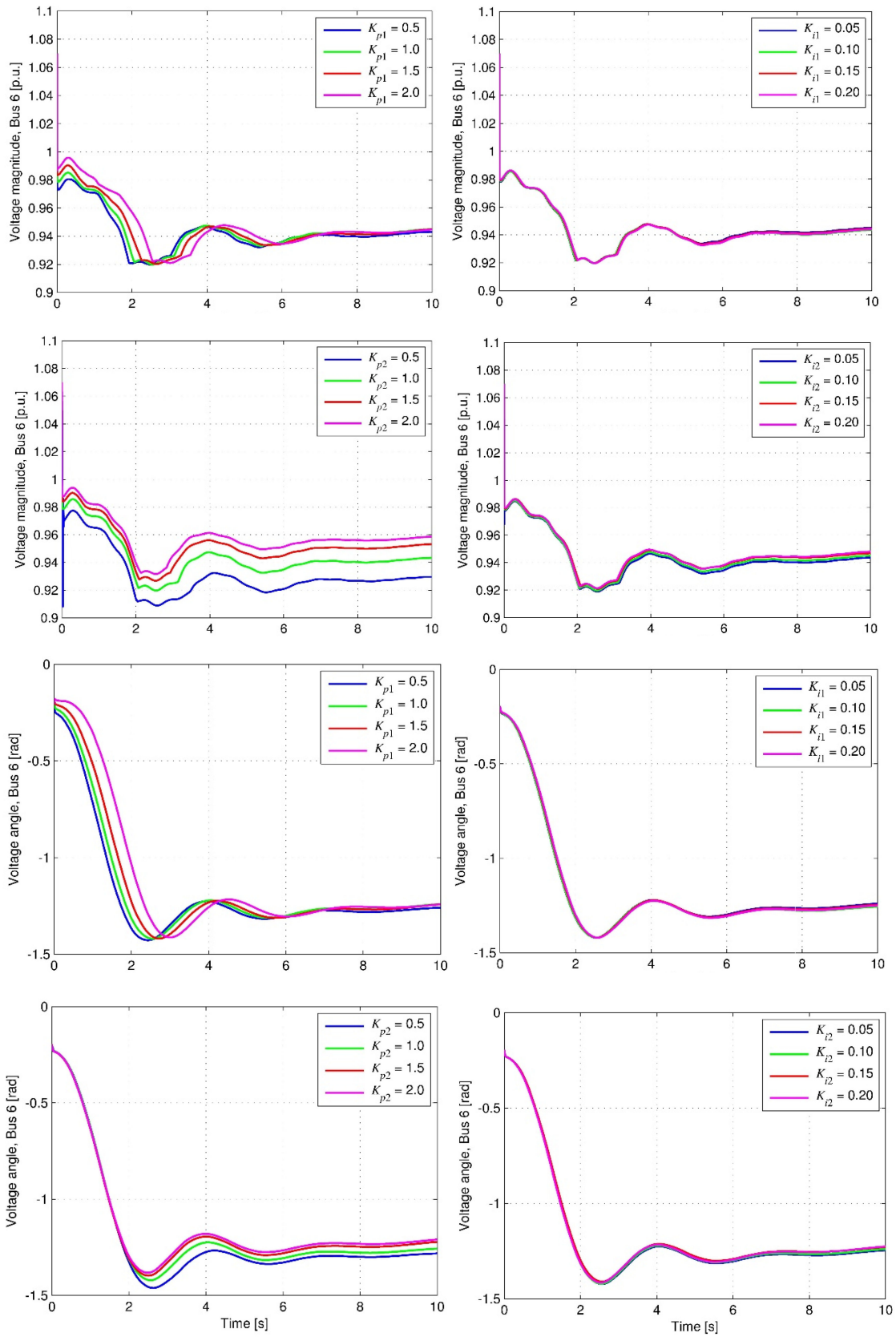


Fig. 4 Time responses of voltage magnitude and angle in DFIG connection bus to parameters of PI controller

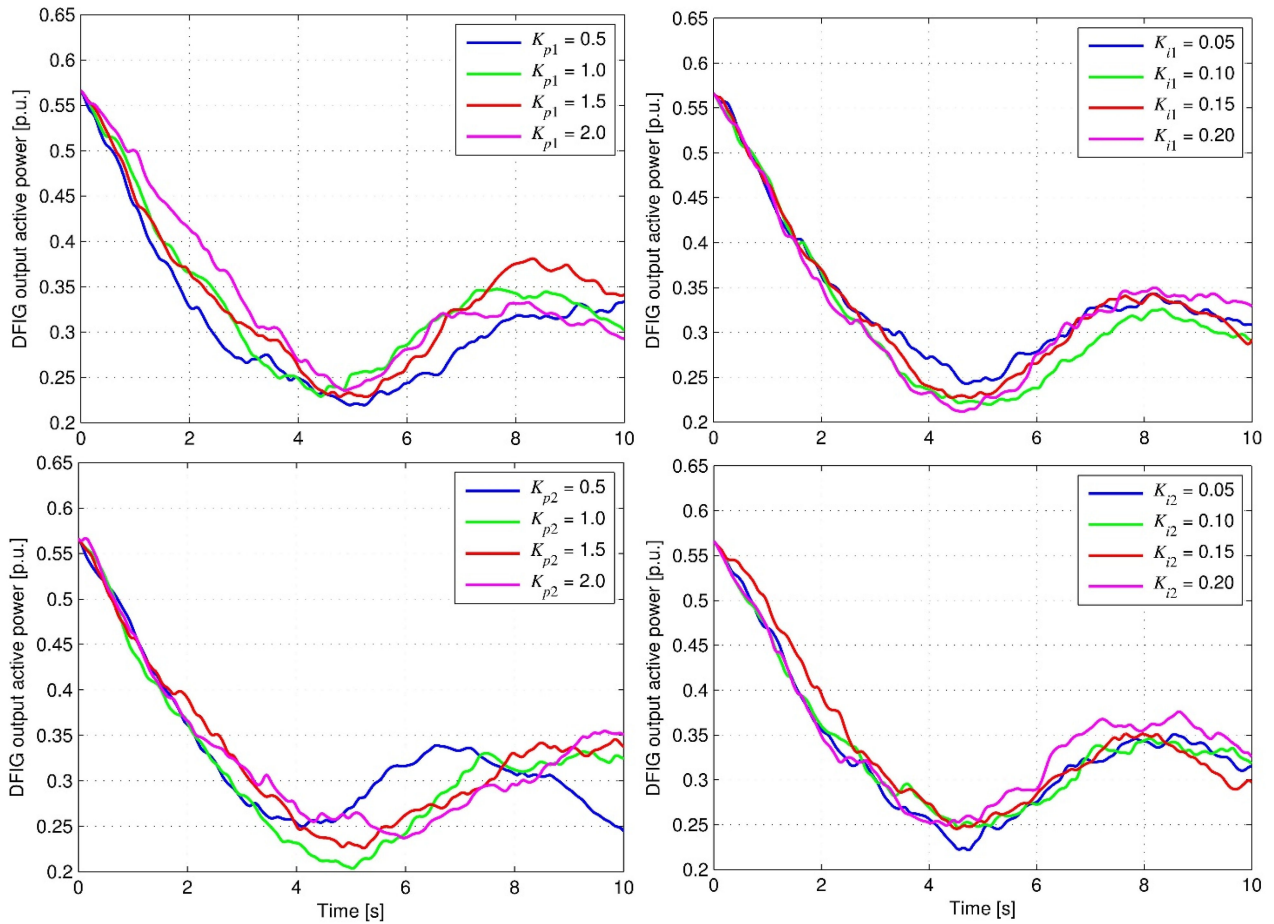


Fig. 5 Time responses of DFIG output active power to parameters of PI controller

8 References

- [1] Andersson, G., Donalek, P., Farmer, R., *et al.*: 'Causes of the 2003 major grid blackouts in North America and Europe, and recommended means to improve system dynamic performance', *IEEE Trans. Power Syst.*, 2005, **20**, (4), pp. 1922–1928
- [2] Kosterev, D.N., Taylor, C.W., Mittelstadt, W.A.: 'Model validation the August 10, 1996 WSCC system outage', *IEEE Trans. Power Syst.*, 1999, **14**, (3), pp. 967–979
- [3] Sanchez-Gasca, J.J., Bridenbaugh, C.J., Bowler, C.E.J., *et al.*: 'Trajectory sensitivity based identification of synchronous generator and excitation system parameters', *IEEE Trans. Power Syst.*, 1988, **3**, (4), pp. 1814–1822
- [4] Benchluch, S.M., Chow, J.H.: 'A trajectory sensitivity method for the identification of nonlinear excitation system models', *IEEE Trans. Energy Convers.*, 1993, **8**, (2), pp. 159–164
- [5] Hiskens, I.A.: 'Nonlinear dynamic model evaluation from disturbance measurement', *IEEE Trans. Power Syst.*, 2001, **16**, (4), pp. 702–710
- [6] Burth, M., Verghese, G.C., Velez-Reyes, M.: 'Subset selection for improved parameter estimation in on-line identification of a synchronous generator', *IEEE Trans. Power Syst.*, 1999, **14**, (1), pp. 218–225
- [7] Cari, E., Alberto, L.F.C.: 'Parameter estimation of synchronous generators from different types of disturbances'. Proc. of the IEEE PES General Meeting, Detroit, MI, USA, July 2011
- [8] Huang, Z., Du, P., Kosterev, D., *et al.*: 'Generator dynamic model validation and parameter calibration using phasor measurements at the point of connection', *IEEE Trans. Power Syst.*, 2013, **28**, (2), pp. 1939–1949
- [9] Choi, B.K., Chiang, H.-D.: 'Multiple solutions and plateau phenomenon in measurement-based load model development: issues and suggestions', *IEEE Trans. Power Syst.*, 2009, **24**, (2), pp. 824–831
- [10] Transtrum, M.K., Sarić, A.T., Stanković, A.M.: 'Information geometry approach to verification of dynamic models in power systems', *IEEE Trans. Power Syst.*, 2017, **PP**, (99), pp. 1–11
- [11] Transtrum, M.K., Sarić, A.T., Stanković, A.M.: 'Measurement-directed reduction of dynamic models in power systems', *IEEE Trans. Power Syst.*, 2017, **32**, (3), pp. 2243–2253
- [12] Transtrum, M.K., Sarić, A.T., Stanković, A.M.: 'Information geometry for model verification in energy systems'. Proc. of the 19th Power Systems Computation Conf. (PSCC), Genoa, Italy, June 2016, pp. 1–7
- [13] Pulgar-Painemal, H.A., Sauer, P.W.: 'Reduced-order model of type-C wind turbine generators', *Electr. Power Syst. Res.*, 2011, **81**, (4), pp. 840–845
- [14] Pulgar-Painemal, H.A., Sauer, P.W.: 'Towards a wind farm reduced-order model', *Electr. Power Syst. Res.*, 2011, **81**, (8), pp. 1688–1695
- [15] Abur, A., Exposito, A.G.: 'Detecting multiple solutions in state estimation in the presence of current magnitude measurements', *IEEE Trans. Power Syst.*, 1997, **12**, (1), pp. 370–375

- [16] Kundur, P.: '*Power system stability and control*' (McGraw-Hill, 1994)
- [17] Transtrum, M.K., Machta, B.B., Sethna, J.P.: 'Why are nonlinear fits to data so challenging?', *Phys. Rev. Lett.*, 2010, **104**, (1), pp. 1–4
- [18] Transtrum, M.K., Machta, B.B., Sethna, J.P.: 'Geometry of nonlinear least squares with applications to sloppy models and optimization', *Phys. Rev. E*, 2011, **83**, (3), pp. 1–35
- [19] Amari, S.-I.: '*Differential-geometrical methods in statistics*' (Springer, 1985)
- [20] Milano, F.: '*Power system modelling and scripting*' (Springer, 2010)
- [21] Ghahremani, E., Kamwa, I.: 'Local and wide-area PMU-based decentralized dynamic state estimation in multi-machine power systems', *IEEE Trans. Power Syst.*, 2016, **31**, (1), pp. 547–562
- [22] Goodman, J., Weare, J.: 'Ensemble samplers with affine invariance', *Commun. Appl. Math. Comput. Sci.*, 2010, **5**, (1), pp. 65–80
- [23] IEC Std 61400-27-1:2015: 'Wind turbines – part 27-1: electrical simulation models – wind turbines', 2015

9 Appendix

Typical DFIG configuration used for renewable energy resources and network model are described in sequel [20, 23].

9.1 Doubly-fed induction generator

Pitch angle control loop, speed/active power control loop, and reactive power control loop are shown in Figs. 6–8, respectively, while differential (motion equation and corresponding control loops) and algebraic equations for DFIG are described, respectively, as

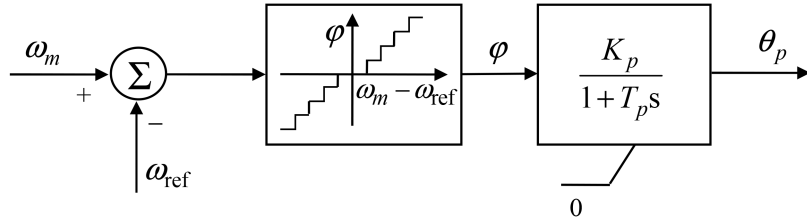


Fig. 6 Pitch angle control loop for DFIG

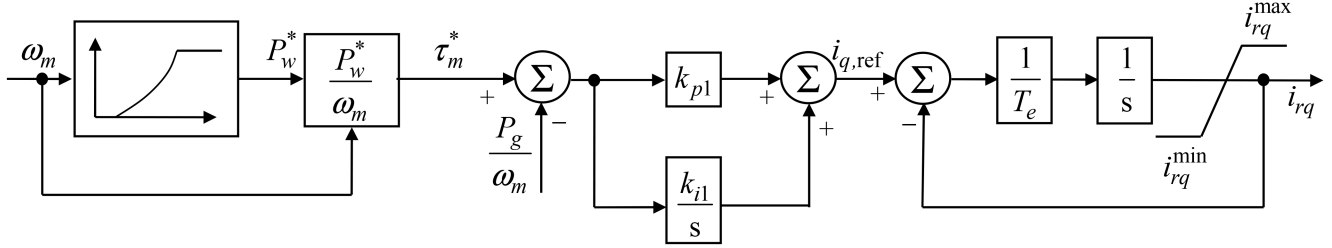


Fig. 7 Speed/active power control loop for DFIG

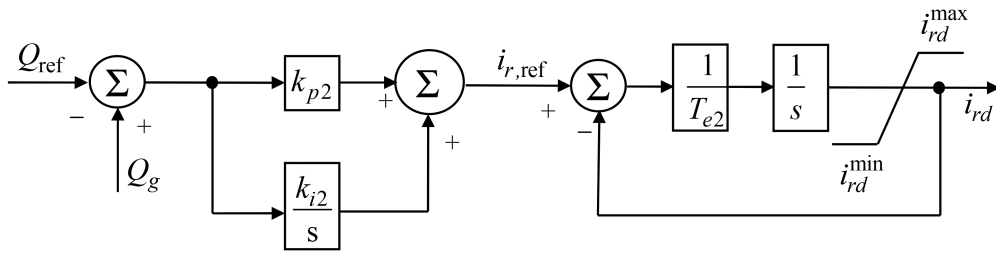


Fig. 8 Reactive power control loop for DFIG

$$f \Rightarrow \begin{cases} \frac{d\omega_m}{dt} = \frac{\tau_m - \tau_e}{2H_m} \\ \frac{d\theta_p}{dt} = \frac{1}{T_p} [K_p \phi(\omega_m - \omega_{ref}) - \theta_p] \\ \frac{dx_1}{dt} = \tau_m^* - \frac{P_g}{\omega_m} = \frac{P_w^*}{\omega_m} - \frac{P_g}{\omega_m} \\ \frac{di_{rq}}{dt} = \frac{1}{T_e} \left[k_{p1} \left(\tau_m^* - \frac{P_g}{\omega_m} \right) + k_{i1} x_1 - i_{rq} \right] \\ \frac{dx_2}{dt} = Q_g - Q_{ref} \\ \frac{di_{rd}}{dt} = \frac{1}{T_{e2}} (i_{r,ref} - i_{rd}) = \frac{1}{T_{e2}} [k_{p2} (Q_g - Q_{ref}) + k_{i2} x_2 - i_{rd}] \end{cases} \quad ; \quad (8)$$

$$g \Rightarrow P_w^*(\omega_m) = \begin{cases} 0, & \text{if } \omega_m < 0.5 \\ 2\omega_m - 1, & \text{if } 0.5 \leq \omega_m \leq 1, \\ 1, & \text{if } \omega_m > 1 \end{cases} \quad (9)$$

where

$$\begin{aligned} \tau_m &= (P_w / \omega_m); \\ \tau_e &= x_\mu (i_{rq} i_{sd} - i_{rd} i_{sq}); \\ P_g &= v_{sd} i_{sd} + v_{sq} i_{sq} + v_{cd} i_{cd} + v_{cq} i_{cq}; \\ Q_g &= v_{sq} i_{sd} - v_{sd} i_{sq} + v_{cq} i_{cd} - v_{cd} i_{cq}; \end{aligned}$$

$$i_{sq} = r_s / (r_s^2 + (x_s + x_\mu)^2) [(x_s + x_\mu) / r_s (-x_\mu i_{rq} + v_{sd}) - x_\mu i_{rd} - v_{sq}];$$

$$i_{sd} = ((x_s + x_\mu) i_{sq} + x_\mu i_{rq} - v_{sd}) / r_s.$$

9.2 Transmission network model

Matrix and complex form of active/reactive bus injection balances is

$$\mathbf{0} = \underline{\mathbf{V}} \underline{\mathbf{Y}}^* \underline{\mathbf{V}}^* - \underline{\mathbf{V}} \underline{\mathbf{I}}(\underline{\mathbf{x}}, \underline{\mathbf{V}}), \quad (10)$$

or algebraic active and reactive bus injection balances, respectively, are

$$P_{inj} = \sum_{j=1}^N [V_i V_j (G_{ij} \cos(\theta_i - \theta_j) + B_{ij} \sin(\theta_i - \theta_j))]; \quad (10a)$$

$$Q_{inj} = \sum_{j=1}^N [V_i V_j (G_{ij} \sin(\theta_i - \theta_j) - B_{ij} \cos(\theta_i - \theta_j))], \quad (10b)$$

where

$$\underline{\mathbf{V}} = \text{diag}\{V_1 \quad V_2 \quad \dots \quad V_N\}; \quad V_i = V_i e^{j\theta_i}$$

$$\underline{\mathbf{Y}} = \underline{\mathbf{G}} + j\underline{\mathbf{B}} - \text{bus admittance matrix.}$$